Determination of 3D-region of interest using digital in-line holography with astigmatic Gaussian beams

Nicolas Verrier, Sébastien Coëtmellec, Marc Brunel, Denis Lebrun

Determination of 3D-region of interest using digital in-line holography with astigmatic Gaussian beams

N. Verrier verrier@coria.fr
Groupe d'Optique et d'Optoélectronique, UMR-6614 CORIA, Av. de l'Université, 76801 Saint-Etienne du Rouvray cedex, France

S. Coëtmellec coetmellec@coria.fr
Groupe d'Optique et d'Optoélectronique, UMR-6614 CORIA, Av. de l'Université, 76801 Saint-Etienne du Rouvray cedex, France

M. Brunel
Groupe d'Optique et d'Optoélectronique, UMR-6614 CORIA, Av. de l'Université, 76801 Saint-Etienne du Rouvray cedex, France

D. Lebrun
Groupe d'Optique et d'Optoélectronique, UMR-6614 CORIA, Av. de l'Université, 76801 Saint-Etienne du Rouvray cedex, France

An experimental method to visualize a 3D-region of interest (ROI) by means of an astigmatic Gaussian beam is proposed. This method allows to reduce the amount of image planes to be reconstructed thus saving computational time. ROI determination is performed without any computational step: particles that are located in the ROI can be distinguished from the others according to the hyperbolic shape of their diffraction pattern. Theoretical location of the ROI is determined by using the ABCD approach proposed in a previous paper [1]. Experimental results are presented. [DOI: 10.2971/jeos.2009.09038]

Keywords: digital holography, astigmatic Gaussian beams, region of interest

1 INTRODUCTION

Digital holography is a recognized optical technique used in a wide range of experiments. For instance fluid mechanics domain benefits from the 3D information given by a digital hologram [2]. Theoretical concepts governing image formation (e.g. influence of pixel mapping, influence of focus, etc.) are now well understood [3]. However, due to its large depth of field, this technique makes it difficult to accurately locate the object along the optical axis without tedious numerical calculation. Depth of focus reduction has been successfully performed in particle field holography [4]. Nevertheless *a priori* knowledge on the particle diameter is needed. Bringing objects to focus is therefore a challenging problem. Automated procedures based on the object spectral, complex or amplitude [5]–[7] signature allow to determine the best focus, making fully automatic hologram treatment possible [8]. Nonetheless these procedures involve heavy calculation (mainly because of the hologram reconstruction) that might be a severe handicap when dealing with a large amount of objects in the volumes. Information about the size and position of objects within the studied volume can be obtained without hologram reconstruction [9, 10], but these methods are either limited by the object density in the sample or give a mean information. One way to overcome this problem is to select only a limited zone to be treated in the total volume. Li et al. propose a numerical method to extract 3D-ROI from digital holograms [11]. By using a fast focus detection algorithm, summing reconstruction kernels at focus positions and segmenting the resulting hologram, the authors manage to extract 3D-ROI information without bulk hologram reconstruction.

Here, we suggest to use digital in-line holography with astigmatic Gaussian beams to select a 3D-ROI, in a pipe flow, directly from the hologram, without any computational step. Recently, an analytical solution of the scalar diffraction produced by an opaque disk, centered on the optical axis, under elliptical astigmatic Gaussian illumination, within the framework of Fresnel approximation, has been proposed [12]. Astigmatism is controlled using a plano-convex cylindrical lens, and particle-to-beam waist position can be determined using the produced diffraction pattern shape. Information about the diffracting object is then easily retrieved using the fractional Fourier transformation (FRFT). These calculations remain valid when we consider an object which not centered on the optical axis [13], making it possible to study flows under astigmatic illumination. Flow study in presence of astigmatism has been successfully performed [1]. Astigmatism is here brought by a cylindrical plano-concave glass pipe. Using Fresnel integral combined with an ABCD formalism, the authors managed to simulate holograms with a good agreement with experimental data. Therefore, it may be possible to control astigmatism within the pipe and above all, to select particles to be reconstructed according to their diffraction pattern shape [1, 12, 13].

2 THEORETICAL LOCATION OF ROI

To perform the particle selection, let us consider the experimental set-up of Figure 1. The distance between the pinhole and the pipe is denoted by z_p. After passing through the clas-

Received June 19, 2009; published July 28, 2009

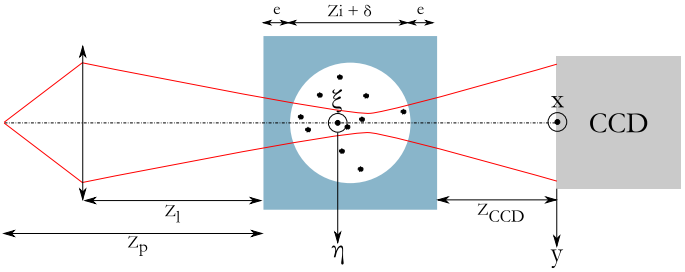

FIG. 1 Schematic representation of the optical set-up (not to scale). Definition of the numerical and experimental parameters.

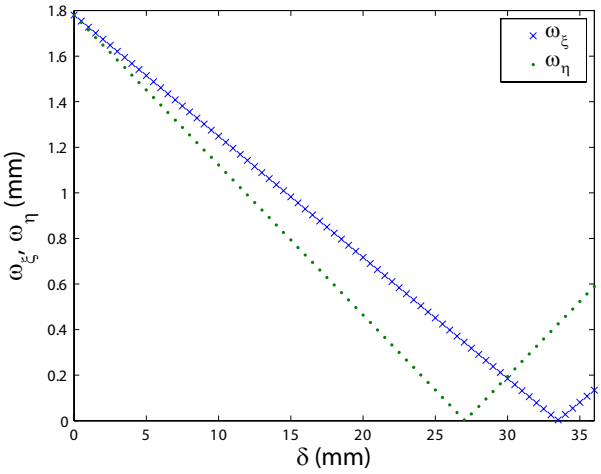

FIG. 2 Evolution of the beam width against position in the pipe. The ROI is located between the beam waists.

sical 50 mm focal length lens, the incident beam propagates to the pipe over a distance denoted z_l. The pipe is modeled as two thick lenses. Their thickness is denoted by e. The opaque objects are located between these two lenses: at a distance δ from the first thick lens and at a distance z_i from the second lens. The 1280×1024 CCD sensor, with a 6.7 μm pixel pitch, is located at a distance z_{CCD} from the pipe and records the intensity distribution of the diffraction pattern. Using the generalized Huygens-Fresnel integral, the intensity distribution in the CCD sensor plane is found to be [1]

$$I(x,y) = \frac{1}{\lambda^2 B_2^x B_2^y}\left(|R|^2 - 2\Re\left\{R\overline{O}\right\} + |O|^2\right). \qquad (1)$$

Here, R is associated with the reference beam and O with the diffracted part of the beam. Their mathematical expressions are

$$R(x,y) = \int_{\mathbb{R}^2} G_1(\xi,\eta)\exp\left[i\frac{\pi}{\lambda B_2^x}\left(A_2^x\xi^2 - 2x\xi + D_2^x x^2\right)\right] \times \exp\left[i\frac{\pi}{\lambda B_2^x}\left(A_2^y\eta^2 - 2y\eta + D_2^y y^2\right)\right] d\xi d\eta \qquad (2)$$

and

$$O(x,y) = \int_{\mathbb{R}^2} G_1(\xi,\eta)\,T(\xi,\eta) \times \exp\left[i\frac{\pi}{\lambda B_2^x}\left(A_2^x\xi^2 - 2x\xi + D_2^x x^2\right)\right] \times \exp\left[i\frac{\pi}{\lambda B_2^y}\left(A_2^y\eta^2 - 2y\eta + D_2^y y^2\right)\right] d\xi d\eta. \qquad (3)$$

Here, $G_1(\xi,\eta)$ denotes the amplitude distribution in the object plane and $T(\xi,\eta)$ is the transfer function of the object. Further explanations about $A_2^{x,y}$, $B_2^{x,y}$, $D_2^{x,y}$, and $I(x,y)$ are given in [1] and in Appendices A and B.

In the set-up of Figure 1, the astigmatism is brought by the cylindrical shape of the pipe. In this case, divergence of the beam is different along ξ- and η-direction. In order to control the astigmatism of the experimental set-up, the beam is focalized in the pipe. Due to the pipe geometry, the beam is successively focused in two waists in the studied volume; one waist along ξ-direction and the other along η-direction. The graph of Figure 2 illustrates this fact. Here, the evolution of the $1/e$ beam width in both directions $\omega_{\xi,\eta}$ is plotted versus the depth position δ in the pipe. Simulation parameters are the following: $z_p = 250$ mm, $z_l = 37$ mm. The pipe considered is a glass made ($n_1 = 1.5$) plano-concave cylinder and is $z_i + \delta = 36$ mm in internal diameter. Its thickness along the optical axis is $e = 12$ mm and it is filled with water ($n_2 = 1.33$). The fact that the beam presents two waists in the pipe is clearly observable from Figure 2; each waist corresponds to a minimum of the $\omega_{\xi,\eta}$ against δ curve. The sagittal and tangential focii are located at $\delta = 28$ mm and $\delta = 33$ mm respectively. For $\delta = 30$ mm the two curves intersect, this is the medial focus. It should be noticed that between the sagittal and tangential focii, the wavefront curvature radii exhibit opposite signs in both directions. Thus objects located within this zone will lead to hyperbolic shaped diffraction patterns, whereas particles located apart from these focii will produce elliptical shaped diffraction patterns [12]. It is hereby possible to distinguish objects located between the two beam waists of objects located elsewhere. In other words, objects located between sagittal and tangential focus will belong to the ROI, whereas other objects will not be processed. Therefore, knowing the $1/e$ beam radii ($\omega_{\xi,\eta}$) within the pipe, it is therefore easy to estimate the ROI volume. The ROI spread over 3.7 mm^3 whereas the recorded volume, which corresponds to the amount of fluid which is illuminated by the beam, is approximately 884 mm^3. We would like to draw attention on the fact that adjusting parameters of the beam within the pipe will modify the ROI volume or the ROI position. For instance, modifying the lens position or focal distance will result in modifying size and position of the ROI.

Theoretical aspects about the ROI determination have been presented. Using the beam astigmatism gives the opportunity to select a small region within which the hologram will be reconstructed. As we aim to reconstruct holograms in the presence of astigmatism, the fractional Fourier transform (FRFT) will be applied to the intensity distribution given in Eq. (1). As a matter of fact, this operator is well adapted to this situation [13]. In Section 3, mathematical expression of the FRFT is recalled and optimal reconstruction parameters are derived.

3 FRACTIONAL FOURIER TRANSFORM ANALYSIS OF THE RECORDED HOLOGRAMS

3.1 Two-dimensional Fractional Fourier Transform

The FRFT is a generalization of the classical Fourier transform. This integral operator is widely applied in signal processing [14]. The FRFT of order $a_x = (2\alpha_x)/\pi$ and $a_y = (2\alpha_y)/\pi$ (for x and y cross section respectively), with $0 \leq |\alpha_x| \leq \pi/2$ and $0 \leq |\alpha_y| \leq \pi/2$, of a two dimensional function $I(x,y)$ is given by,

$$\mathcal{F}_{\alpha_x,\alpha_y}[I(x,y)](x_a,y_a) = \int_{\mathbb{R}^2} N_{\alpha_x}(x,x_a)\, N_{\alpha_y}(y,y_a) I(x,y)\, dx\, dy \quad (4)$$

where the kernel of the fractional operator is defined by

$$N_{\alpha_p}(x,x_a) = C(\alpha_p) \exp\left(i\pi \frac{x^2+x_a^2}{s_p^2 \tan\alpha_p}\right) \exp\left(-\frac{i2\pi x_a x}{s_p^2 \sin\alpha_p}\right) \quad (5)$$

and

$$C(\alpha_p) = \frac{\exp(-i(\frac{\pi}{4}\mathrm{sign}(\sin\alpha_p) - \frac{\alpha_p}{2}))}{|s_p^2 \sin\alpha_p|^{1/2}}. \quad (6)$$

Here, $p = x, y$. The coefficient $C(\alpha_p)$ ensure the energy conservation in every fractional domains. Generally, s_p is considered as a normalization constant, but its value can be linked to the experimental set-up [13]. In this case, $s_p^2 = N_p^{px} \times \delta_p^2$. The number of samples is N_p^{px} in both intensity distribution $I(x,y)$ and fractional domain. δ_p is the sampling period along the two axes of the image.

3.2 Optimal fractional orders

FRFT reconstruction consists in canceling quadratic phases contained by the intensity distribution of the hologram. The intensity distribution is given Eq. (1). We can notice that the terms $|R|^2$ and $|O|^2$ do not contain any quadratic phases. Thus, they will not be treated by FRFT. The quadratic phases to be analyzed are contained in $\Re\{R\overline{O}\}$. As revealed by Eqs. (35) and (40), this term is composed of a linear chirp modulated by a sum of complex Gaussian functions. Compensating this chirp will result in reconstructing the hologram.

The quadratic phases can be determined from Eqs. (35) and (40),

$$\varphi = \frac{\pi}{\lambda}\left[\left(\frac{M_x - D_2^x}{B_2^x}\right)x^2 + \left(\frac{M_y - D_2^y}{B_2^y}\right)y^2\right] \quad (7)$$

thus $\Re\{R\overline{O}\}$ can be written as

$$\Re\{R\overline{O}\} = |R\overline{O}|\cos(\varphi). \quad (8)$$

The quadratic phase term contained in the FRFT kernel, denoted φ_a, is given by

$$\varphi_a = \pi\left(\frac{\cot\alpha_x}{s_x^2}x^2 + \frac{\cot\alpha_y}{s_y^2}y^2\right) \quad (9)$$

To reconstruct the hologram, the FRFT is applied to the intensity distribution given Eq. (1),

$$\mathcal{F}_{\alpha_x,\alpha_y}[I(x,y)] \propto \mathcal{F}_{\alpha_x,\alpha_y}\left[|R|^2 + |O|^2\right] - 2\mathcal{F}_{\alpha_x,\alpha_y}\left[|R\overline{O}|\cos\varphi\right]. \quad (10)$$

We would like to draw attention on the fact that the terms $|R|^2$ and $|O|^2$ contain no linear chirps. They will not influence the optimal orders to be determined. Only the second term will be useful for image reconstruction.

By noting that $2\cos\varphi = \exp(-i\varphi) + \exp(i\varphi)$, Eq. (10) becomes

$$\begin{aligned}\mathcal{F}_{\alpha_x,\alpha_y}[I(x,y)] \propto\ & \mathcal{F}_{\alpha_x,\alpha_y}\left[|R|^2 + |O|^2\right] \\ & - \left\{C(\alpha_x)\, C(\alpha_y) \int_{\mathbb{R}^2} |R\overline{O}| \exp[i(\varphi_a - \varphi)] \right. \\ & \left. \times \exp\left[-i2\pi\left(\frac{x_a x}{s_x^2 \sin\alpha_x} + \frac{y_a y}{s_y^2 \sin\alpha_y}\right)\right] dxdy\right\} \\ & - \left\{C(\alpha_x)\, C(\alpha_y) \int_{\mathbb{R}^2} |R\overline{O}| \exp[i(\varphi_a + \varphi)] \right. \\ & \left. \times \exp\left[-i2\pi\left(\frac{x_a x}{s_x^2 \sin\alpha_x} + \frac{y_a y}{s_y^2 \sin\alpha_y}\right)\right] dxdy\right\}. \end{aligned} \quad (11)$$

Reconstruction of the hologram is performed when one of the quadratic phase terms is brought to zero. In this case,

$$\varphi_a \pm \varphi = 0. \quad (12)$$

Thus, the optimal fractional orders α_x^{opt} and α_y^{opt} defined from Eqs. (7), (9) and (12) take the values

$$\begin{aligned}\alpha_x^{opt} &= \arctan\left[\mp\frac{B_2^x \lambda}{s_x^2\left(M_x - D_2^x\right)}\right] \\ \alpha_y^{opt} &= \arctan\left[\mp\frac{B_2^y \lambda}{s_y^2\left(M_y - D_2^y\right)}\right]. \end{aligned} \quad (13)$$

4 EXPERIMENTAL RESULTS

To illustrate the interest of our idea, an experimental hologram is recorded. The optical set-up of Figure 1 is considered. The distance between the 15 μm pinhole and the pipe is fixed to $z_p = 250$ mm and a 50 mm focal length lens is positioned $z_l = 37$ mm before the pipe. The glass made pipe is filled with water and illuminated with an He-Ne laser ($\lambda = 632.8$ nm). 50 μm in diameter latex beads are injected in the ROI and the intensity distribution produced by these is recorded on a CCD sensor without objective lens. Distance between the CCD sensor and the pipe is $z_{CDD} = 18$ mm. According to the experimental parameters, the ROI will be located between $\delta = 28$ mm and $\delta = 33$ mm (position of the sagittal and tangential focus respectively). The intensity distribution obtained under these conditions is presented in Figure 3. We can realize from the hologram that elliptical and hyperbolic fringe patterns are simultaneously observed. Elliptical patterns are due to particles that are located outside the ROI, i.e. $\delta \in [0\text{ mm}; 28\text{ mm}[\cap]33\text{ mm}; 36\text{ mm}]$, whereas hyperbolic

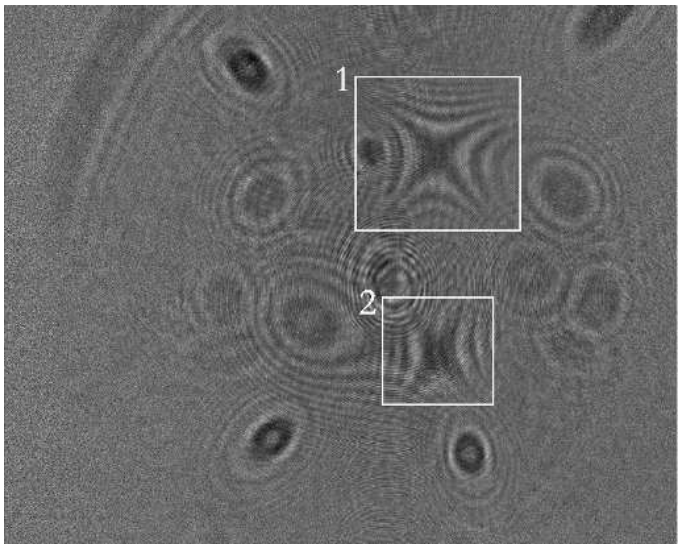

FIG. 3 Experimental hologram of 50 μm latex beads recorded with $z_p = 250$ mm, $z_l = 37$ mm, and $z_{CCD} = 18$ mm. Two particles are in the ROI.

shaped diffraction patterns are due to particles that are in the ROI, i.e $\delta \in [28\,\text{mm}; 33\,\text{mm}]$. Thus by simply looking at the hologram of Figure 3, without using complex shape recognition procedure, we can notice that two particles (labeled "1" and "2") are located in the ROI. Information about these two particles can be retrieved by reconstructing the hologram only in the ROI, thus reducing the amount of data to be processed.

Reconstruction of this hologram can be performed using FRFT [14]. In fact, FRFT is a really efficient reconstruction operator when dealing with astigmatic holograms [1, 12, 13]. Numerical refocusing on particle "1" is proposed Figure 4(a). Reconstructed image of the particle is obtained by adjusting the fractional orders of the FRFT within the range defined, from Eq. (13), by the ROI position. Particle is considered in focus when the best contrast (determined by plotting intensity profiles along particle axis) between the image of the latter and the background is reached. To refocus on particle "1", a FRFT of orders $a_x = 0.71$, $a_y = -0.8$ is performed. It should be noted that the FRFT orders have opposite signs. This is due to the fact that, within the ROI, wavefront curvature radii exhibit opposite signs. Refocusing on particle "2" (see Figure 4(b)) is possible with $a_x = 0.61$, $a_y = -0.88$.

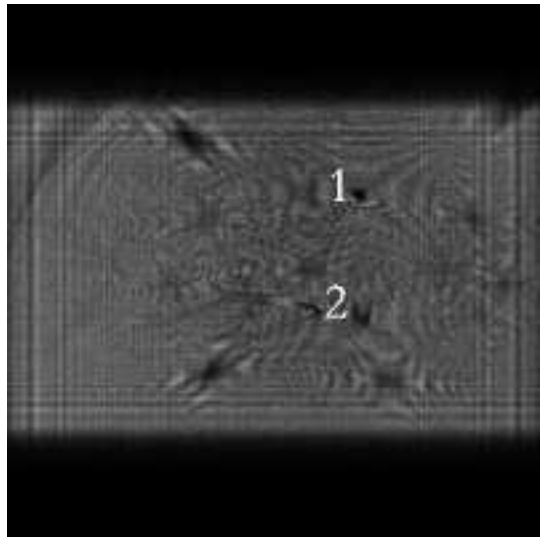

(a)

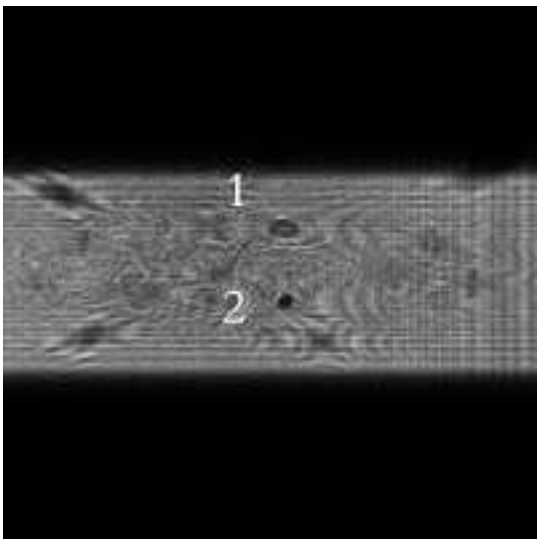

(b)

FIG. 4 FRFT reconstruction of Figure 3 with (a) $a_x = 0.71$ and $a_y = -0.8$ (b) $a_x = 0.61$ and $a_y = -0.88$

5 CONCLUSION

In summary, we have proposed and demonstrated a convienent method to select a 3D-ROI within an hologram. This achievement is of great interest as it does not need bulk computational treatment; the 3D-ROI selection is experimentally performed by using the astigmatic properties of pipe flows. Working within a limited 3D-ROI is a good way to reduce the amount of data to be treated or to refine hologram processing in a limited zone. Experimental implementation has been performed showing the possibility of optically selecting a 3.7 mm^3 ROI within a 884 mm^3 studied volume. Finally, particles contained in the ROI have been reconstructed using the fractional Fourier transform.

ACKNOWLEDGEMENTS

This work was supported by the Agence Nationale de la Recherche (Edition 2007 du programme BLANC: "VIVE3D - Vélocimétrie Instantanée Volumique pour les Ecoulements tridimensionnels").

A TRANSFER MATRICES OF THE OPTICAL SYSTEM

Each part of an optical system can be represented by a matrix. Using this principle, we can build a set of matrices corresponding to our experiment (Figure 1). After passing through the pinhole, the beam propagates in free space over a distance

z_p–z_l. The associated $M_{z_p-z_l}$ matrix is

$$M_{z_p-z_l} = \begin{pmatrix} 1 & z_p - z_l \\ 0 & 1 \end{pmatrix}. \quad (14)$$

The beam is then focalized by a thin spherical lens. The focal distance of this lens is denoted by f. The associated transfer matrix M_{lens} is

$$M_{lens} = \begin{pmatrix} 1 & 0 \\ -\frac{n_0}{f} & 1 \end{pmatrix}. \quad (15)$$

After the thin lens, the beam propagates, over a distance z_l, to the pipe. The matrix M_{z_l}, associated with this step, is given by

$$M_{z_l} = \begin{pmatrix} 1 & z_l \\ 0 & 1 \end{pmatrix}. \quad (16)$$

Then the beam is refracted at the interface between free space and glass ($n_1 = 1.5$). The curvatures along both directions are R_{x1} and R_{y1}. $M_{R_{x1}}$, $M_{R_{y1}}$ matrices along x and y axis are

$$M_{R_{x1}} = \begin{pmatrix} 1 & 0 \\ \frac{n_0-n_1}{R_{x1}} & 1 \end{pmatrix} \quad M_{R_{y1}} = \begin{pmatrix} 1 & 0 \\ \frac{n_0-n_1}{R_{y1}} & 1 \end{pmatrix}. \quad (17)$$

After refraction, the beam propagates in glass ($n_1 = 1.5$). For this step,

$$M_e = \begin{pmatrix} 1 & \frac{e}{n_1} \\ 0 & 1 \end{pmatrix}. \quad (18)$$

Next step is the refraction of the beam at the interface between glass and the medium inside the pipe (refractive index n_2). Curvatures R_{x2} and R_{y2} in x and y direction are given by

$$M_{R_{x2}} = \begin{pmatrix} 1 & 0 \\ \frac{n_1-n_2}{R_{x2}} & 1 \end{pmatrix} \quad M_{R_{y2}} = \begin{pmatrix} 1 & 0 \\ \frac{n_1-n_2}{R_{y2}} & 1 \end{pmatrix}. \quad (19)$$

We are now in the pipe. To reach the object, we have to propagate over δ,

$$M_\delta = \begin{pmatrix} 1 & \frac{\delta}{n_2} \\ 0 & 1 \end{pmatrix}. \quad (20)$$

Doing the same over z_i permit us to reach the output of the pipe,

$$M_{z_i} = \begin{pmatrix} 1 & \frac{z_i}{n_2} \\ 0 & 1 \end{pmatrix}. \quad (21)$$

After a refraction at the interface (curvatures R_{x3} and R_{y3}) between the medium with refractive index n_2 and glass,

$$M_{R_{x3}} = \begin{pmatrix} 1 & 0 \\ \frac{n_2-n_1}{R_{x3}} & 1 \end{pmatrix} \quad M_{R_{y3}} = \begin{pmatrix} 1 & 0 \\ \frac{n_2-n_1}{R_{y3}} & 1 \end{pmatrix}, \quad (22)$$

a propagation in glass ($n_1 = 1.5$),

$$M_e = \begin{pmatrix} 1 & \frac{e}{n_1} \\ 0 & 1 \end{pmatrix}, \quad (23)$$

a refraction at the interface (curvature R_{x4} and R_{y4}) between glass ($n_1 = 1.5$) and free space,

$$M_{R_{x4}} = \begin{pmatrix} 1 & 0 \\ \frac{n_1-n_0}{R_{x4}} & 1 \end{pmatrix} \quad M_{R_{y4}} = \begin{pmatrix} 1 & 0 \\ \frac{n_1-n_0}{R_{y4}} & 1 \end{pmatrix} \quad (24)$$

and free space propagation over z_{CCD},

$$M_{z_{CCD}} = \begin{pmatrix} 1 & z_{CCD} \\ 0 & 1 \end{pmatrix}, \quad (25)$$

the whole ABCD system is described.

B AMPLITUDE DISTRIBUTIONS $R(x,y)$ AND $O(x,y)$

In Appendix A each part of our optical system has been represented with transfer matrices. Using this formalism allows us, under paraxial conditions, to deal with propagation of a Gaussian point source through the pipe.

Intensity distribution of the diffraction pattern in the CCD sensor plane is determined by considering two matrix systems $M_1^{x,y}$ and $M_2^{x,y}$.

$M_1^{x,y}$ is composed of five steps; propagation in free space over $z_l - z_p$, beam focalization, propagation in free space over z_l, propagation through the first thick lens, propagation in a medium of refractive index n_2 over δ. These steps are characterized by two transfer matrices,

$$\begin{aligned} M_1^{x,y} &= M_\delta \times M_{L_1}^{x,y} \times M_{z_l} \times M_{lens} \times M_{z_p-z_l} \\ &= \begin{pmatrix} A_1^{x,y} & B_1^{x,y} \\ C_1^{x,y} & D_1^{x,y} \end{pmatrix}. \end{aligned} \quad (26)$$

$M_2^{x,y}$ is also composed of three steps; propagation in a medium of refractive index n_2 over z_i, propagation through the second thick lens, propagation in free space over z. Transfer matrices for this system are,

$$M_2^{x,y} = M_{z_{CCD}} \times M_{L_2}^{x,y} \times M_{z_i} = \begin{pmatrix} A_2^{x,y} & B_2^{x,y} \\ C_2^{x,y} & D_2^{x,y} \end{pmatrix}. \quad (27)$$

Thanks to Eqs. (17)–(19) one can build the transfer matrices of the first thick lens,

$$\begin{aligned} M_{L_1}^x &= M_{R_{x2}} \times M_e \times M_{R_{x1}} \\ M_{L_1}^y &= M_{R_{y2}} \times M_e \times M_{R_{y1}}. \end{aligned} \quad (28)$$

By using the same method for the second lens, we obtain

$$\begin{aligned} M_{L_2}^x &= M_{R_{x4}} \times M_e \times M_{R_{x3}} \\ M_{L_2}^y &= M_{R_{y4}} \times M_e \times M_{R_{y3}}. \end{aligned} \quad (29)$$

B.1 Propagation through $M_1^{x,y}$

Propagation through $M_1^{x,y}$ is calculated using the generalized Huygens-Fresnel integral,

$$G_1(\xi,\eta) = \frac{\exp\left(i\frac{2\pi}{\lambda}E_1\right)}{i\lambda\sqrt{B_1^x B_1^y}} \int_{\mathbb{R}^2} G(\mu,\nu) \times \exp\left[i\frac{\pi}{\lambda B_1^x}\left(A_1^x\mu^2 - 2\xi\mu + D_1^x\xi^2\right)\right] \times \exp\left[i\frac{\pi}{\lambda B_1^y}\left(A_1^y\nu^2 - 2\eta\nu + D_1^y\eta^2\right)\right] d\mu d\nu. \quad (30)$$

After analytical developments of Eq. (30), the complex amplitude distribution in the object plane is

$$G_1(\xi,\eta) = \frac{\exp\left(i\frac{2\pi}{\lambda}E_1\right)}{i\lambda\sqrt{B_1^x B_1^y}} K_1^x K_1^y \exp\left[-\left(\frac{\xi^2}{\omega_{1_x}^2} + \frac{\eta^2}{\omega_{1_y}^2}\right)\right] \times \exp\left[-i\frac{\pi}{\lambda}\left(\frac{\xi^2}{R_{1_x}} + \frac{\eta^2}{R_{1_y}}\right)\right] \quad (31)$$

with $K_1^{x,y}$ given by

$$K_1^{x,y} = \left(\frac{\pi\omega^2}{1 - iA_1^{x,y}\frac{\pi\omega^2}{\lambda B_1^{x,y}}}\right)^{1/2}, \quad (32)$$

$\omega_{1_{x,y}}$ and $R_{1_{x,y}}$ are respectively the beam radii and the wavefront curvature in the particle plane. Their mathematical expressions are

$$\omega_{1_{x,y}} = \left(\frac{\lambda B_1^{x,y}}{\pi\omega}\right)\left[1 + \left(A_1^{x,y}\frac{\pi\omega^2}{\lambda B_1^{x,y}}\right)^2\right]^{1/2}$$
$$R_{1_{x,y}} = -B_1^{x,y}\left[D_1^{x,y} - \frac{A_1^{x,y}\left(\frac{\pi\omega^2}{\lambda B_1^{x,y}}\right)^2}{1 + \left(A_1^{x,y}\frac{\pi\omega^2}{\lambda B_1^{x,y}}\right)^2}\right]^{-1}. \quad (33)$$

B.2 Propagation through $M_2^{x,y}$

Propagation to the CCD sensor plane is given by the following integral,

$$G_2(x,y) = \frac{\exp\left(i\frac{2\pi}{\lambda}E_2\right)}{i\lambda\sqrt{B_2^x B_2^y}} \int_{\mathbb{R}^2} G_1(\xi,\eta)\left[1 - T(\xi,\eta)\right] \times \exp\left[i\frac{\pi}{\lambda B_2^x}\left(A_2^x\xi^2 - 2x\xi + D_2^x x^2\right)\right] \times \exp\left[i\frac{\pi}{\lambda B_2^y}\left(A_2^y\eta^2 - 2y\eta + D_2^y y^2\right)\right] d\xi d\eta. \quad (34)$$

The integral of Eq. (34) can be split into two integrals R and O associated with the reference beam and the diffracted beam respectively. Their expressions are given in Eqs. (2) and (3).

B.2.1 Amplitude distribution $R(x,y)$

R is associated with the reference wave. After analytical developments of Eq. (2), the amplitude distribution R is

$$R(x,y) = \frac{\exp\left(i\frac{2\pi}{\lambda}E_1\right)}{i\lambda\sqrt{B_1^x B_1^y}} K_1^x K_1^y K_2^x K_2^y \times \exp\left[-\frac{\pi}{\lambda}\left(\frac{N_x}{B_2^x}x^2 + \frac{N_y}{B_2^y}y^2\right)\right] \times \exp\left[i\frac{\pi}{\lambda}\left(\frac{M_x}{B_2^x}x^2 + \frac{M_y}{B_2^y}y^2\right)\right] \quad (35)$$

where

$$M_{x,y} = D_2^{x,y} + \frac{\left(\frac{\pi\omega_{1_{x,y}}^2}{\lambda B_2^{x,y}}\right)^2\left(\frac{B_2^{x,y}}{R_{1_{x,y}}} - A_2^{x,y}\right)}{1 + \left(\frac{\pi\omega_{1_{x,y}}^2}{\lambda B_2^{x,y}}\right)^2\left(\frac{B_2^{x,y}}{R_{1_{x,y}}} - A_2^{x,y}\right)^2}$$
$$N_{x,y} = \frac{\frac{\pi\omega_{1_{x,y}}^2}{\lambda B_2^{x,y}}}{1 + \left(\frac{\pi\omega_{1_{x,y}}^2}{\lambda B_2^{x,y}}\right)^2\left(\frac{B_2^{x,y}}{R_{1_{x,y}}} - A_2^{x,y}\right)^2} \quad (36)$$

and

$$K_2^{x,y} = \left[\frac{\pi\omega_{1_{x,y}}^2}{1 + i\frac{\pi\omega_{1_{x,y}}^2}{\lambda B_2^{x,y}}\left(\frac{B_2^{x,y}}{R_{1_{x,y}}} - A_2^{x,y}\right)}\right]^{1/2}. \quad (37)$$

B.2.2 Amplitude distribution $O(x,y)$

O is the amplitude of the diffracted wave. We define $\omega_{1_{x,y_{eq}}}$ and $R_{1_{x,y_{eq}}}$

$$\frac{1}{\omega_{1_{x_{eq}}}^2} = \frac{1}{\omega_{1_x}^2} + \frac{\Re\{B_k\}}{b^2}$$
$$\frac{1}{\omega_{1_{y_{eq}}}^2} = \frac{1}{\omega_{1_y}^2} + R_{ell}^2\frac{\Re\{B_k\}}{b^2} \quad (38)$$

and

$$\frac{1}{R_{1_{x_{eq}}}} = \frac{1}{R_{1_x}} + \frac{\Im\{B_k\}\lambda}{\pi b^2}$$
$$\frac{1}{R_{1_{y_{eq}}}} = \frac{1}{R_{1_y}} + R_{ell}^2\frac{\Im\{B_k\}\lambda}{\pi b^2} \quad (39)$$

to simplify notations. It should be noted that $\Re$ and $\Im$ stand for real and imaginary part respectively. Thus O becomes

$$O(x,y) = \frac{\exp\left(i\frac{2\pi}{\lambda}E_1\right)}{i\lambda\sqrt{B_1^x B_1^y}} K_1^x K_1^y \exp\left[i\frac{\pi}{\lambda}\left(\frac{D_2^x}{B_2^x}x^2 + \frac{D_2^y}{B_2^y}y^2\right)\right] \times \sum_{k=1}^{N} A_k K_2^{x_{eq}} K_2^{y_{eq}} \exp\left[-\frac{\pi}{\lambda}\left(\frac{N_{x_{eq}}}{B_2^x}x^2 + \frac{N_{y_{eq}}}{B_2^y}y^2\right)\right] \times \exp\left[i\frac{\pi}{\lambda}\left(\frac{M_{x_{eq}}}{B_2^x}x^2 + \frac{M_{y_{eq}}}{B_2^y}y^2\right)\right] \quad (40)$$

with

$$M_{x,y_{eq}} = \frac{\left(\frac{\pi\omega^2_{1_{x,y_{eq}}}}{\lambda B_2^{x,y}}\right)^2 \left(\frac{B_2^{x,y}}{R_{1_{x,y_{eq}}}} - A_2^{x,y}\right)}{1 + \left(\frac{\pi\omega^2_{1_{x,y_{eq}}}}{\lambda B_2^{x,y}}\right)^2 \left(\frac{B_2^{x,y}}{R_{1_{x,y_{eq}}}} - A_2^{x,y}\right)^2}$$

$$N_{x,y_{eq}} = \frac{\frac{\pi\omega^2_{1_{x,y_{eq}}}}{\lambda B_2^{x,y}}}{1 + \left(\frac{\pi\omega^2_{1_{x,y_{eq}}}}{\lambda B_2^{x,y}}\right)^2 \left(\frac{B_2^{x,y}}{R_{1_{x,y_{eq}}}} - A_2^{x,y}\right)^2} \qquad (41)$$

and

$$K_2^{x,y_{eq}} = \left[\frac{\pi\omega^2_{1_{x,y_{eq}}}}{1 + i\frac{\pi\omega^2_{1_{x,y_{eq}}}}{\lambda B_2^{x,y}}\left(\frac{B_2^{x,y}}{R_{1_{x,y_{eq}}}} - A_2^{x,y}\right)}\right]^{1/2}. \qquad (42)$$

References

[1] N. Verrier, S. Coëtmellec, M. Brunel, and D. Lebrun, "Digital in-line holography in thick optical systems: application to visualization in pipes" Appl. Opt. **47**, 4147–4157 (2008).

[2] N. Salah, G. Godard, D. Lebrun, P. Paranthoën, D. Allano, and S. Coëtmellec, "Application of multiple exposure digital in-line holography for particle tracking in a Bénard-von Kármán vortex flow" Meas. Sci. Technol. **19**, 074001 (2008).

[3] P. Picart, and J. Leval, "General theoretical formulation of image formation in digital Fresnel holography" J. Opt. Soc. Am. A **25**, 1744–1761 (2008).

[4] W. Yang, A. B. Kostinski, and R. A. Shaw, "Depth-of-focus reduction for digital in-line holography of particle fields" Opt. Lett. **30**, 1303–1305 (2005).

[5] W. Li, N. C. Loomis, Q. Hu, and C. S. Davis, "Focus detection from digital in-line holograms based on spectral l_1 norms" J. Opt. Soc. Am. A **24**, 3054–3062 (2007).

[6] J. de Jong, and H. Meng, "Digital holographic particle validation via complex wave" Appl. Opt. **46**, 7652–7661 (2007).

[7] F. Dubois, C. Schockaert, N. Callens, and C. Yourassowsky, "Focus plane detection criteria in digital holography microscopy by amplitude analysis" Opt. Express **14**, 5895–5908 (2006).

[8] E. Malkiel, J. N. Abras, and J. Katz, "Automated scanning and measurements of particle distributions within a holographic reconstructed volume" Meas. Sci. Technol. **15**, 601–612 (2004).

[9] L. Onural, and M. T. Özgen, "Extraction of three-dimensional object-location information directly from in-line holograms using Wigner analysis" J. Opt. Soc. Am. A **9**, 252–260 (1992).

[10] L. Denis, C. Fournier, T. Fournel, C. Ducottet, and D. Jeulin, "Direct extraction of the mean particle size from a digital hologram" Appl. Opt. **45**, 944–952 (2006).

[11] W. Li, N. C. Loomis, Q. Hu, and C. Davis, *Rapid extraction of 3D regions of interest from digital holograms* (MTS/IEEE Oceans 2007 Conference, Vancouver, 29 September–4 October 2007).

[12] F. Nicolas, S. Coëtmellec, M. Brunel, D. Allano, D. Lebrun, and A. J. E. M. Janssen, "Application of the fractional Fourier transformation to digital holography recorded by an elliptical, astigmatic Gaussian beam" J. Opt. Soc. Am. A **22**, 2569–2577 (2005).

[13] N. Verrier, S. Coëtmellec, M. Brunel, D. Lebrun, and A. J. E. M. Janssen, "Digital in-line holography with an elliptical, astigmatic Gaussian beam: wide-angle reconstruction" J. Opt. Soc. Am. A **25**, 1459–1466 (2008).

[14] H. M. Ozaktas, Z. Zalevsky, and M.A. Kutay, *The Fractional Fourier Transform: with Applications in Optics and Signal Processing* (John Wiley & Sons, 2001).